

This article was downloaded by: [Kamran Mohseni]

On: 02 April 2013, At: 11:03

Publisher: Taylor & Francis

Informa Ltd Registered in England and Wales Registered Number: 1072954 Registered office: Mortimer House, 37-41 Mortimer Street, London W1T 3JH, UK



Advanced Robotics

Publication details, including instructions for authors and subscription information:
<http://www.tandfonline.com/loi/tadr20>

Passive mitigation of roll stall for low aspect ratio wings

Matt Shields^a & Kamran Mohseni^b

^a Department of Mechanical & Aerospace Engineering, University of Florida, 32611-6250, Gainesville, FL, USA

^b Mechanical & Aerospace Engineering Department and Electrical & Computer Engineering Department, Institute for Networked Autonomous Systems, University of Florida, 32611-6250, Gainesville, USA

Version of record first published: 02 Apr 2013.

To cite this article: Matt Shields & Kamran Mohseni (2013): Passive mitigation of roll stall for low aspect ratio wings, *Advanced Robotics*, DOI:10.1080/01691864.2013.778941

To link to this article: <http://dx.doi.org/10.1080/01691864.2013.778941>

PLEASE SCROLL DOWN FOR ARTICLE

Full terms and conditions of use: <http://www.tandfonline.com/page/terms-and-conditions>

This article may be used for research, teaching, and private study purposes. Any substantial or systematic reproduction, redistribution, reselling, loan, sub-licensing, systematic supply, or distribution in any form to anyone is expressly forbidden.

The publisher does not give any warranty express or implied or make any representation that the contents will be complete or accurate or up to date. The accuracy of any instructions, formulae, and drug doses should be independently verified with primary sources. The publisher shall not be liable for any loss, actions, claims, proceedings, demand, or costs or damages whatsoever or howsoever caused arising directly or indirectly in connection with or arising out of the use of this material.

FULL PAPER

Passive mitigation of roll stall for low aspect ratio wings

Matt Shields^a and Kamran Mohseni^{b*}

^aDepartment of Mechanical & Aerospace Engineering, University of Florida, Gainesville, FL 32611-6250, USA;

^bMechanical & Aerospace Engineering Department and Electrical & Computer Engineering Department, Institute for Networked Autonomous Systems, University of Florida, Gainesville 32611-6250, USA

(Received 10 September 2012; final version received 26 November 2012)

This investigation addresses an issue with the lateral stability and control of Micro Aerial Vehicles (MAVs) which is created by the presence of ‘roll stall’ and its effects on the aircraft’s stability derivatives. This behavior is a result of the developing tip vortex asymmetry of a low aspect ratio (LAR) wing in sideslip which creates an asymmetric spanwise load and a resulting roll moment. Experimental wind tunnel results indicate that roll stall produces a roll stability derivative, $C_{l,\beta}$, for both the MAV models tested as well as canonical tapered flat wing cases; furthermore, even at small sideslip angles, the cross-coupled derivative $C_{l,\alpha}$ links the longitudinal aerodynamics and the lateral loads of LAR wings, effects which are not present for large aircraft. The roll stall creates nonlinearities in lateral loads in an angle of attack regime in which the lift variation is linear; thus, control techniques for MAVs must consider the fact that lateral and longitudinal equations of motion can not necessarily be linearized about the same equilibrium flight conditions. Finally, the addition of winglets below the plane of the wing is seen to reduce $C_{l,\beta}$ by at least 50% in some cases, as well as essentially eliminating the derivative for a taper ratio of $\lambda = 0.25$. This provides a passive control technique which can potentially be employed to significantly reduce the lateral instabilities of MAVs.

Keywords: micro aerial vehicles; roll stall; lateral stability and control; wind tunnel testing

1. Introduction

The recent prevalence of Micro Aerial Vehicles (MAVs) for sensor networking applications has given rise to the development of a wide array of aircraft designs; fixed, flapping, and rotary wing MAVs have all been developed and flown by various institutions for a number of missions. [1–5] Despite the achievements of building a flying vehicle (such as the Prototype Interactive PERformance [PIPER] MAV developed by the authors and shown in Figure 1), the nature of the aerodynamic loading of MAVs is still not well understood as the flowfield around the wing is dominated by viscous effects and separation at the leading edge [6–11] as well as three-dimensional (3D) velocity fields created by the propagation of the tip vortex along the inherently short wingspan. [12–14] These flow phenomena are known to affect the surface pressure distributions, stall characteristics, load asymmetry, and unsteady behavior of MAV wings. [14–21] Naturally, this invalidates many of the assumptions which are typically made in linearized control theory; i.e., laminar flow, high aspect ratios, and the decoupling of lateral and longitudinal loads. [22] As a result, the problem of MAV control does not have a simple solution akin to conventional aircraft as the effects of these nonlinearities must be understood, modeled, and incorporated in

any efficient flight controller. The purpose of this paper is to experimentally quantify unconventional effects on lateral loading caused by sideslip perturbations and to describe the impact of these loads on the stability and control of low aspect ratio (LAR) wings.

Much of the existing work on MAV control has focused on developing autonomous swarms of vehicles for rapid dispersion and characterization of a wide area of interest, such as chemical or nuclear leaks. [23,24] Despite the increasingly sophisticated algorithms used for controlling the fleet of vehicles, [25] a fundamental lack of understanding of the vehicle dynamics still remains and limits the ability of these control techniques to model the behavior of the individual MAVs. While some work has been done to characterize the flight envelope and implement simple controllers for various MAVs, [3,4,26] an inherent limitation of these techniques has been the assumption that conventional aerodynamic models can be applied to the unique flow regime associated with LAR fliers. This can be reasonably effective for delta wing vehicles with wingspans on the order of 1 m [25,27]; however, for MAVs with complex geometries and wingspans on the order of 10 cm, the propagation of tip vortices over the surface of the wing drastically affects the aerodynamic loading and results in high values of α_{stall} and

*Corresponding author. Email: mohseni@ufl.edu



Figure 1. PIPER MAV developed by the group; photo from December 2008.

$C_{L,max}$. [13,14] Furthermore, recent results obtained by the authors demonstrate the existence of a ‘roll stall’ phenomenon for LAR wings in which angle of attack sweeps conducted at increasing sideslip angles show a linearly increasing value of the roll moment followed by a stall event qualitatively similar to a lift polar. [28,29] The magnitude of the roll polar was found to be significant and the resulting roll stability derivative ($C_{l,\beta}$) was typically outside the range of good handling qualities for conventional aircraft. [22] This phenomena was of particular interest as the models tested in the study were flat plate wings with no dihedral, camber, or vertical tail surfaces, which are conventionally the major contributors to $C_{l,\beta}$ [22]; instead, the creation of the roll moment was attributed to the spanwise variations in loading on the yawed wing created by the developing asymmetry of the tip vortices. As the sideslip angle increases, the tip vortex emanating from the downstream wingtip is mostly convected away from the wing whereas the upstream wingtip is located above the surface of the model. For a negative sideslip angle, this creates a strongly positive roll moment. Smokewire visualization was used to confirm this behavior; results are shown in Figure 2 for a flat plate wing with a taper ratio of $\lambda = 0.25$. This unique flow phenomena is not modeled by conventional aerodynamic theory and must be further investigated to efficiently control a LAR aircraft. In this study, the significance of roll stall for the PIPER MAV will be quantified and additional experiments are undertaken to assess methods of passively mitigating the adverse effects of roll stall by reducing the magnitude of the $C_{l,\beta}$ derivative.

This manuscript is organized as follows: first, the experimental setup including the wind tunnel, positioning system, force balance, and data acquisition methods will be described in Section 2. Sections 3.1 and 3.2 present and describe the static lateral and longitudinal loads measured in the investigation. Static stability derivatives resulting from these measurements, including the existence of cross-coupled derivatives assumed to be negligible for higher aspect ratio fliers, are presented in Sections 3.3 and 3.4.

Finally, the impact of the results on the control of MAVs is discussed in Section 4 and compared with the stability derivatives of conventional aircraft.

2. Experimental setup

2.1. Wind tunnel and force balance

The low Reynolds number wind tunnel (the Prototunnel) used for this study has been described in detail in previous work by the authors. [14] The open-circuit, closed-jet tunnel is capable of velocities up to 20 m/s with low freestream turbulence intensities on the order of 0.1% resulting in only minor hysteresis. The Prototunnel is outfitted with the Model Positioning System (MPS) which can actuate a test model in roll, pitch, yaw, and plunge in the test section. Aerodynamic loads are measured using the Micro Loading Technology (MLT) force balance, a six-component internal strain gauge balance.

2.2. Experimental procedure

The data acquisition and analysis procedure is similar to other low Reynolds number studies of static aerodynamic loads. [13,14] MAVs typically fly in Reynolds number regime between 5×10^4 and 1×10^5 in which the static aerodynamic loads do not vary significantly. [13,14] As a result, in this investigation, only a Reynolds number of 7.5×10^4 is tested; this nondimensional parameter is defined as:

$$Re = \frac{\rho U_0 c}{\mu}, \quad (1)$$

in which Re is the Reynolds number, ρ is the air density, U_0 is the freestream velocity, c is the root chord of the model, and μ is the dynamic viscosity.

The coordinate system used for the investigation is shown in Figure 3. Results are presented in the body axes of the model being tested, with the roll moment positive when the MAV rolls its left wingtip upwards. The sideslip angle is defined to be negative when there is a component of the freestream velocity vector in the $+y_b$ direction.

The testing procedure was as follows: a model was mounted on the MPS and set at a desired sideslip angle ($\beta = 0^\circ, -5^\circ, -10^\circ, -15^\circ, \text{ or } -20^\circ$). Only testing negative sideslip angles inherently assumes symmetry about the $x-z$ plane, which was verified using several test cases. A range of angles of attack was selected in which the model would reach lift stall; these angles were measured prior to the test using a digital protractor. A ‘zero reference data set’ was then collected with the wind off at each incidence angle tested in order to subtract out the inertial loads measured by the MLT balance. The test was then repeated with the wind

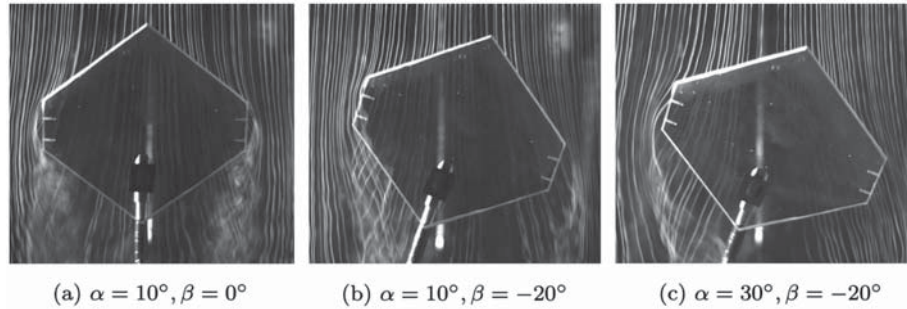


Figure 2. Smokewire visualization for a flat plate wing with $AR=1$ and $\lambda = 0.25$ at $\beta = 0^\circ$ and -20° for $Re = 7.5 \times 10^4$.

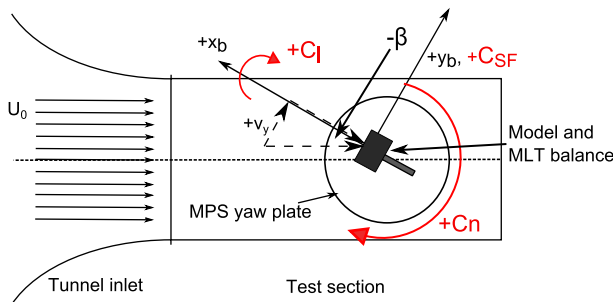


Figure 3. Coordinate axes and definition of sideslip angle.

on to measure the aerodynamic loads of the models. Results were all found to be identically repeatable within the bounds of experimental error.

2.3. Test models

The test models used in this investigation included a modified version of the PIPER (without propeller or avionics) and a series of simple flat plates, the former of which demonstrates the specific aerodynamic loads of the MAV developed by the authors and the latter of which are used as canonical test cases which are representative of the behavior of a wide variety of wings without the influence of the tails or fuselage. The relevant geometric properties of the PIPER pictured in Figure 1 are listed in Table 1. The MAV is fabricated entirely from pre-impregnated carbon fiber. The wing and fuselage are formed ('laid up') as a single part in order to increase the rigidity of the airframe and thus to improve its strength for landings. The fuselage is approximately rectangular with a width of 3.2cm and a length of 8.9cm; it is incident with the leading edge of the wing and is tapered at the front to reduce drag. Each tail surface is laid up individually and is glued to the top surface of the wing at an inclination of approximately 8° to the centerline of the MAV. The airfoil used for the wing utilizes a cambered/reflexed design with the maximum camber and reflex occurring at 19% and 82% of the chord,

respectively. The resultant pitch stability of the wing makes a horizontal tail unnecessary. The net mass of the flight model of the PIPER (including avionics, servos and propeller) is 80g.

The dimensions of the canonical flat plate models tested are displayed in Table 2; the tapered wings have 0% camber and were fabricated from acrylic. The wings have the cross section of a thin plate and, therefore, eliminate the effects of camber and wing dihedral on the aerodynamic loads. The leading edge is elliptic with a 5:1 ratio of the major and minor axes, which diminishes the size of the leading edge stagnation point. While previous work by the authors has investigated both rectangular and tapered wing planforms,[14] in this study only the tapered wings were tested to better represent the swept leading edge common to MAVs. The main goal of this investigation is to attempt to reduce the roll moment created by the tip vortex propagation over the wingtips; to accomplish this, winglets can be attached to the flat plate wings to impede the formation of the tip vortices. The winglets are fabricated in a similar manner to the wings themselves; the leading edge is tapered and the thickness is the same as that of the wings (0.4cm). The winglets are simple rectangles with the same length as the tip chord of the wing. They can be mounted to the wing at either the bottom or the top of the winglet so that the attachment extends above or below the wing, respectively.

2.4. Data acquisition

To measure the loads at each incidence angle, 2^{14} samples were collected over a 4-sec sampling period, which is sufficient to allow unsteady flow phenomena (i.e., vortex shedding) to be temporally averaged out. A 4th order lowpass Butterworth filter was set at 1kHz to eliminate high frequency noise. Strain gauge readings were iteratively converted to physical loads using a technique based on the AIAA strain gauge standard.[30] Wind tunnel blockage effects were corrected according to the techniques presented by Rae and Pope [31]. Bias errors were computed prior to the tests by measuring the loads of known weights and were found to be under 3% for the roll moment axis and

Table 1. PIPER MAV geometric properties.

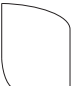


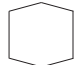
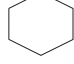
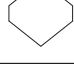
Wing		Vertical tail surfaces	
b,cm.	20.3	Max height,cm.	8.9
c,cm.	17.3	Max width,cm.	7.6
Dihedral angle,deg.	8	Incidence angle,deg.	~8
Surface area,cm. ²	290	Surface area,cm. ²	64.5
Max camber,cm.	1.1 @ .19c	Side profile of tail geometry	
Max reflex,cm.	0.2 @ .82c	Tail position relative to wing	
Inverse Zimmerman planform (top view)			

Table 2. Flat plate model dimensions.

AR	c_{root} , cm.	c_{tip} ,cm.	b,cm.	t,cm.	λ	Winglet dim., cm.	Diagram
1	15.2	11.4	15.2	0.4	0.75	11.4×3.8×0.4	
1	15.2	7.6	15.2	0.4	0.5	7.6×3.8×0.4	
1	15.2	3.8	15.2	0.4	0.25	3.8×3.8×0.4	

under 1% for all other axes. The large number of samples taken and the 16-bit resolution of the A/D converter result in negligible values of random error and quantization error. With the exceptions of a few post-stall data points, 95% confidence bounds were within 1% of the sample mean.

3. Results

3.1. MAV loads

The presence of the ‘roll stall’ observed on low aspect ratio, flat plate wings signifies the influence that the short wingspan of MAVs has on the aerodynamic loading and stability of these vehicles. The complexity of the flow regime for an actual vehicle will naturally be compounded by geometric features such as the planform, wing camber, and presence of the tail surfaces; the associated influence of the tip vortices and the resulting impact on roll stall is not currently known. Thus, it is necessary to conduct similar tests as in [14] to determine how roll stall is manifested on an actual vehicle as opposed to a canonical test case. It should be noted that the PIPER MAV (Figure 1) tested in this paper is not expected to precisely replicate the aerodynamic loading of all MAVs, which differ significantly in design parameters; however, it is representative of many features common to these vehicles and can be considered a qualitative indication of the trends experienced by MAVs.

3.1.1. Test results

The PIPER was mounted on the MPS at increasing sideslip angles and swept between angles of attack of $-15^\circ \leq \alpha \leq 30^\circ$ at a Reynolds number of 7.5×10^4 ; the tests were repeated with the tail surfaces removed to assess the impact of the vertical tails on the loading. A selection of results are shown in Figures 4 and 5; only the longitudinal loads for the MAV with tails attached are shown as the additional geometry did not significantly affect the lift, drag or pitching moment. All moments are defined about the quarter root chord of the model.

The plots for the longitudinal loads (C_L , C_D , C_M) in Figure 4 typically show little variation for all sideslip angles tested; the exception to this is the increase in C_D for the higher sideslip angles due to the greater profile drag. The largest variation is observed in the roll moment polars, which vary significantly between sideslip angles for both the tail on and off configurations. Figure 5(a) shows a gradually increasing roll moment coefficient up to an angle of attack of $\alpha \sim 12^\circ$, at which point an apparent roll stall occurs for the full PIPER model. The tailless MAV (Figure 5(b)) creates a larger slope leading up to a stall at the same angle of attack but a reduced $C_{l,max}$. A moderate nonzero slope is noticeable at a sideslip angle of zero; this can be attributed to leading edge asymmetries creating a spanwise varying stagnation point.[17,28] This affects the formation of both the tip vortices and the leading edge separation bubble and

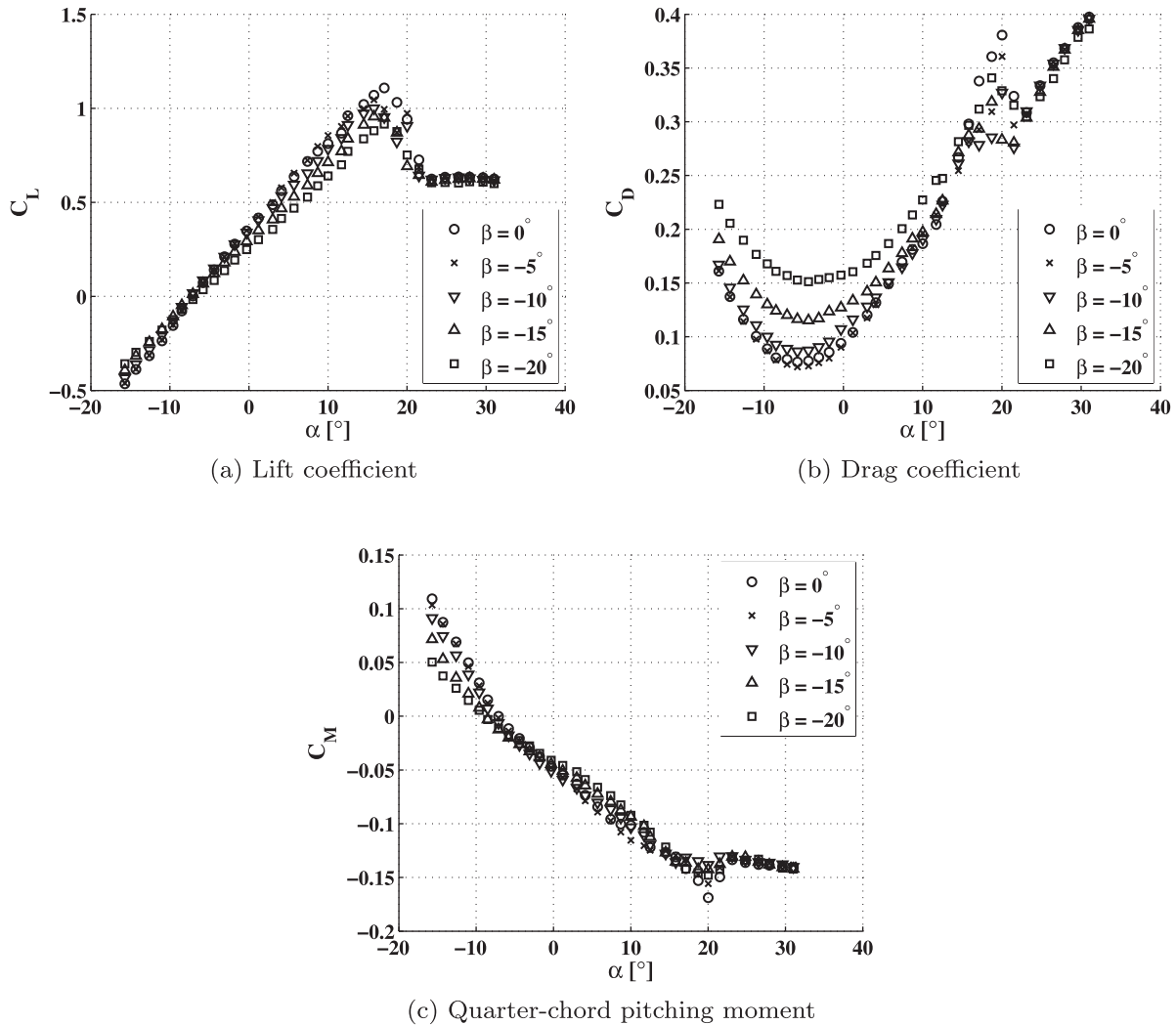


Figure 4. Longitudinal loads for the PIPER MAV in sideslip at $Re = 7.5 \times 10^4$.

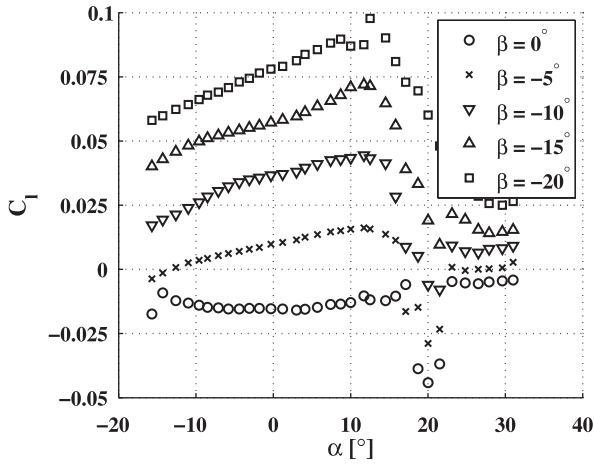
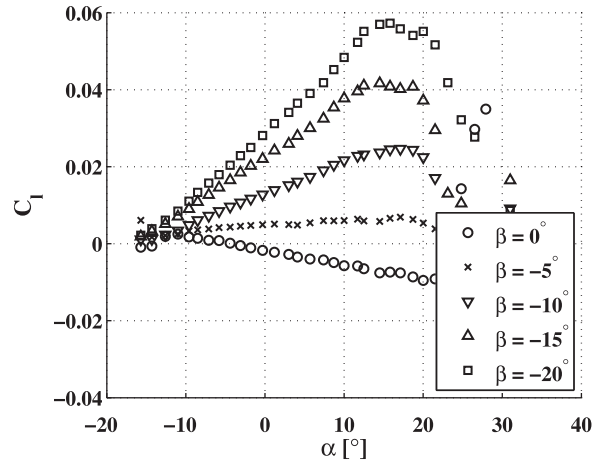
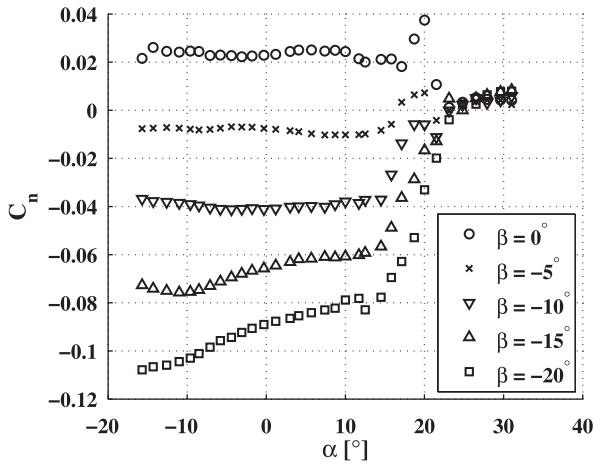
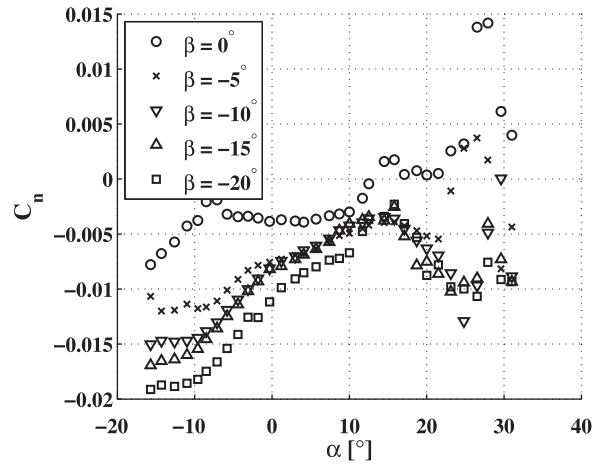
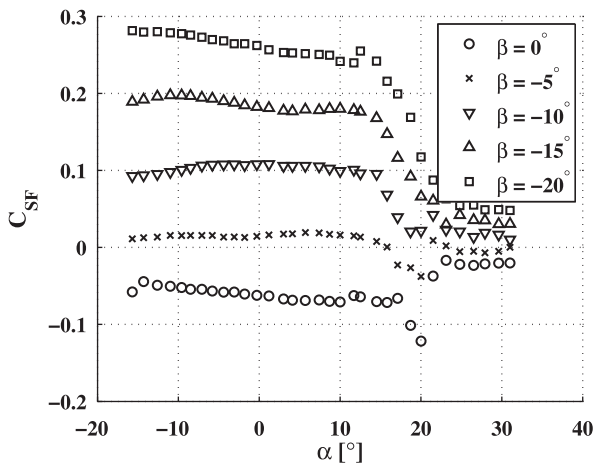
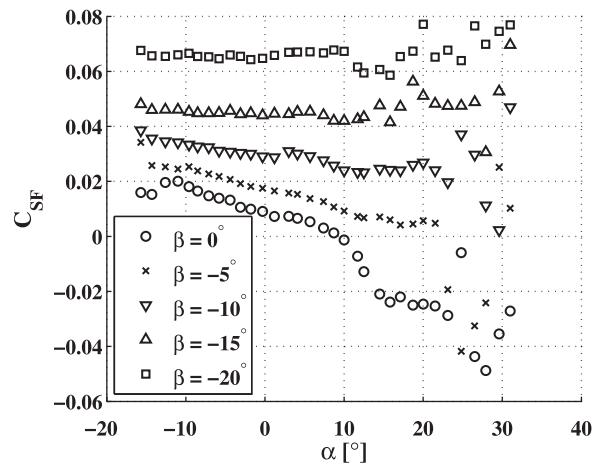
has been found to create small, but nonzero, roll moments with zero sideslip or bank angles [17]; the results from this study show that the asymmetric tip vortices create small lateral loads for both the PIPER and the flat plate wings at zero sideslip angle. Finally, it is interesting to note that the presence of vertical tails (Figure 5(a)), even at $\beta = 0^\circ$, results in enough of an interaction that the slope approaches zero but the nominal value of C_l is negative. This indicates the complex, interactive nature of the flow around a MAV wing creates many competing effects which need to be carefully characterized.

The inference to be drawn from Figure 5(a) and (b) is that, while the tail surfaces contribute significantly to the roll moment at low angles of attack, the spanwise loading created by the asymmetric tip vortices becomes dominant at angles of attack above $\alpha = 10^\circ$. Although the incident flow on the vertical tails inherently creates a positive roll moment about the x -axis, the stall event present at all sideslip angles around $\alpha = 12^\circ$ creates a significant nonlinearity in lateral

loading. The lift polar (Figure 4(a)) shows a reasonably linear slope in the same range of angle of attack, which suggests that this may be potential linearization point for the aerodynamic loading; however, when considering the roll moment, it is clear that the lateral loading experiences significant nonlinearities at the same trim condition. Thus, the nature of lateral and longitudinal loads for a MAV indicates that while one component can be easily modeled with a linear approximation, the same model is not necessarily applicable to forces on other axes. Roll stall creates an adverse loading condition which rapidly changes the lateral forces experienced by a LAR wing; thus, further investigation into mitigation techniques is desirable.

3.2. Canonical test cases

The results shown in Section 3.1 indicate that roll stall is indeed prevalent on actual MAV wings, similar to the flat plate wings tested in [28,29]. Control methods for these vehicles

(a) C_l for the MAV with tails(b) C_l for the MAV without tails(c) C_n for the MAV with tails(d) C_n for the MAV without tails(e) C_{SF} for the MAV with tails(f) C_{SF} for the MAV without tailsFigure 5. Lateral loads for PIPER MAV models in sideslip at $Re=7.5 \times 10^4$.

must naturally incorporate the effects of this phenomena in order to correctly model lateral stability characteristics. In addition to simply understanding and incorporating these effects, a reduction in the large magnitude of the roll moment created by the tip vortex asymmetry may simplify the nature of MAV control. In this preliminary study, winglets are added to the flat plate geometry with the goal of passively reducing the roll moment of a wing in sideslip.

3.2.1. Baseline cases: tapered flat wings

Before describing the results of the modified tapered wings, it is illustrative to show the results for tapered planforms with no winglets and zero bank angle as a baseline comparison; plots for $\lambda = 0.25, 0.5, 0.75$ are shown in Figures 6 and 7. This data is modified from results taken from [28]. Some key points to note are the relatively large magnitudes of the roll polar and the clear roll stall regime for the $\lambda = 0.75$ case. This reduction in roll moment near $\alpha = 22^\circ$ is due to the disruption of the upstream tip vortex by the adverse pressure gradient along the wing at high angles of attack. As seen in Figure 2(c), the attached vortex no longer has a coherent core and, as a result of the weakened vortex, the induced roll moment is decreased. At $\lambda = 0.5$, the interaction between the tip vortices and the leading edge vortex prevents the development of roll stall and at $\lambda = 0.25$ the magnitude is significantly decreased due to the small wingtip and resulting reduced impact of tip vortices. The side force and yaw moment are approximately constant over the range of angles of attack tested, although they are seen to vary with sideslip angle (and the associated variation in induced drag created by the asymmetric tip vortices).[28] While the effects of yaw moment and, to a lesser extent, side force due to sideslip are of interest for MAV control, the purpose of this investigation is to reduce the magnitude of the roll moment slope and, thus, the value of the $C_{l,\beta}$ stability derivative which is most responsible for static lateral stability.[22] Data presented in the following sections will refer back to Figures 6 and 7.

3.2.2. Effect of winglets on lateral loading

Winglets have traditionally been added to conventional wings to reduce the impact of tip vortices on the induced drag of the aircraft; however, as shown in this paper, they can also be used to disrupt the formation of the upstream tip vortex and reduce the significance of roll stall for LAR wings. To investigate this, endplates were mounted to the wingtips of the tapered wings in configurations both above and below the plane of the wing itself. The same battery of tests were then conducted at the same Reynolds number of 7.5×10^4 so that the influence of the winglets on the lateral loading could be assessed. It should be noted that the longitudinal loads of the tapered wings with and without winglets were reported by the authors in [14]. A sample of

results are shown in Figures 8 and 9 for taper ratios of 0.5 and 0.75, respectively.

The first point to note from the results is that the yaw moment and side force are consistently negative and positive (respectively). The sign of the loads is consistent whether the winglets are above or below the wing, and can be attributed to the incident flow upon the winglets. When the wing is set at a negative sideslip angle, a normal flow incident upon the winglets exists; this creates a force in the $+y$ direction along the wing corresponding to the positive side force. It can be assumed that this flow is reasonably uniform along the chord of the wing and the force is symmetric about the half chord; thus, the yaw moment about the quarter chord of the wing is nonzero and negative.

The roll moment is more significant from a control perspective; while the magnitudes are typically similar to the yaw moment, it is important to recognize that the moments of inertia about the roll axis (I_{xx}) are much smaller than about the other axes.[3,4] This makes the roll moment more significant for MAVs than for conventional transport aircraft (in which I_{xx} is more comparable with the other inertia components due to the fuel storage in the wings [32]). Thus, the roll moment will have a greater effect on the response of a MAV than the yaw moment. Comparison of the data in Figure 8(a) and (b), as well as Figure 9(a) and (b), indicates that the shape of the curves are antisymmetric. This is to be expected as the geometry is essentially reversed; the winglets down configuration at a negative angle of attack mirrors the winglets up configuration at a positive angle of attack. In the context of MAV control, the winglets down configuration is of the most interest. When compared to Figure 6, it is clear that while a roll stall event still occurs, the magnitude of the roll moment is drastically decreased. The presence of the winglets below the wing disrupts the formation of tip vortices and reduces the associated roll moment. Above-wing winglets are less effective at this disruption, and in fact increase the magnitude of the roll moment in some cases. Figures 8(a) and 9(a) show promising results in reducing the magnitude of the roll moment and thus simplifying MAV control techniques.

While the characteristics of the roll polar are significantly different between the winglets on and off configurations, it is interesting to note that the longitudinal loads are not.[14] This is an important consideration in roll stall mitigation, as the modification of the wing geometry can be applied to reduce the roll moment in sideslip perturbations without adversely affecting the lifting characteristics of the wing.

3.3. Stability derivatives due to angle of attack

Using the experimental results presented in the previous section, it is simple to compute the static stability derivatives of the PIPER MAV and of the flat plate wings. As variations due to bank angle ϕ were found to be negligible (as expected because the wing still sees the same flow component), $\partial/\partial\phi$

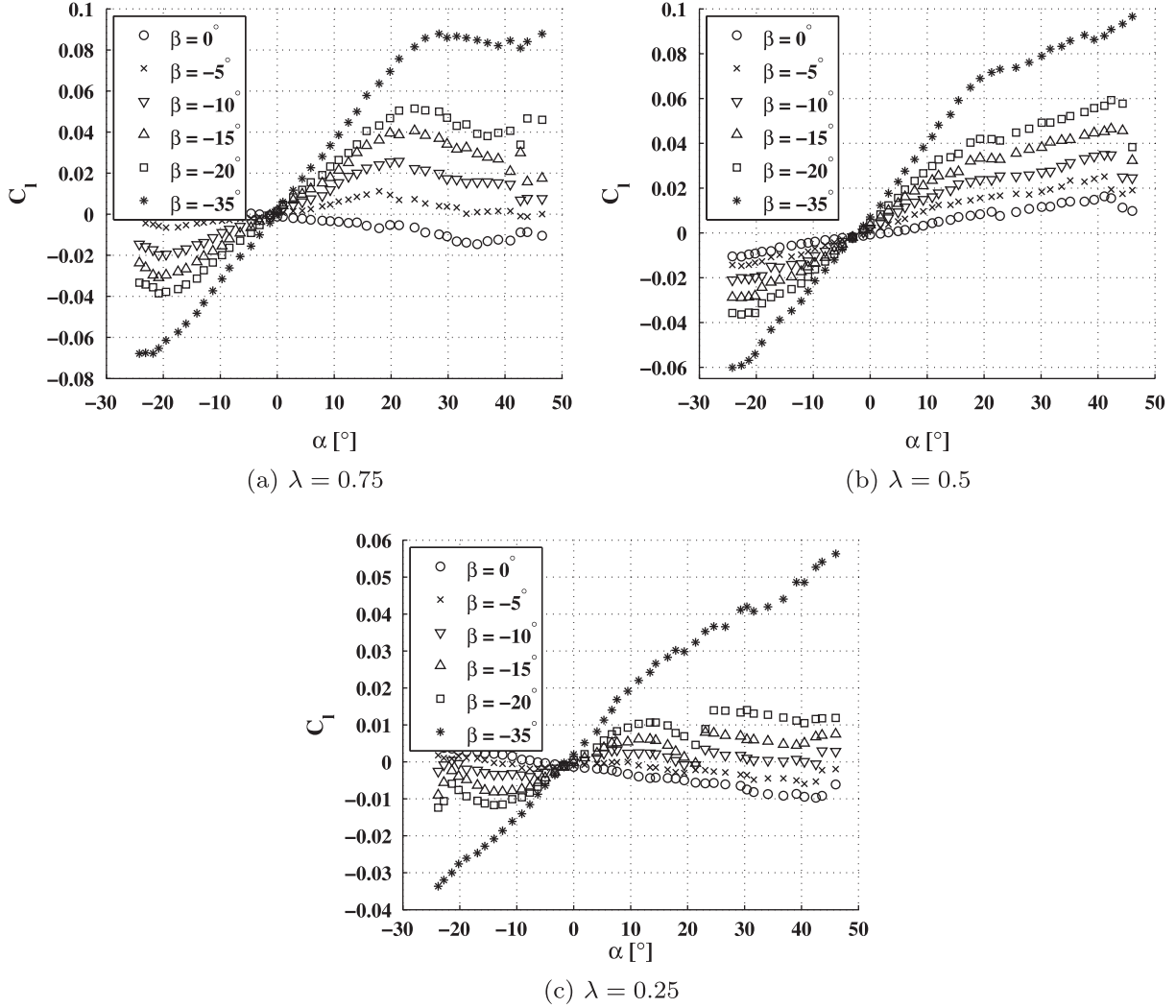


Figure 6. Roll moment coefficient for tapered flat plate wings with AR=1 in sideslip at $Re=7.5 \times 10^4$.

derivatives were considered to be zero. The purpose of evaluating the stability derivatives of the test models is to assess the possibility of implementing a linear controller; naturally, this requires determining an equilibrium flight condition about which the load F can be represented by a first order Taylor series expansion:

$$C_F(\alpha, \beta, \dots) = C_{F_0}(\alpha_0, \beta_0, \dots) + C_{F,\alpha}(\alpha - \alpha_0) + C_{F,\beta}(\beta - \beta_0) + \dots, \quad (2)$$

in which $C_{F,x}$ represents the stability derivative of F with respect to the state variable x . The assumption that the lateral and longitudinal loads are decoupled is typically invoked, making it possible to set derivatives such as $C_{l,\alpha} = 0$ for a large aircraft. The purpose of the current investigation is not to undertake a full stability analysis of the PIPER MAV (or other geometries), but rather to examine the experimentally obtained derivatives and to use the results to determine if

the first-order linear approximation given by Equation 2 is valid. As such, an equilibrium angle of attack of $\alpha_{\text{trim}} = 10^\circ$ (the nominal cruise angle of the PIPER) is selected and static derivatives are evaluated over a domain of $5^\circ \leq \alpha_{\text{trim}} \leq 15^\circ$, which corresponds to a reasonable flight envelope for a MAV. Ideally, a constant value for the $\partial/\partial\alpha$ derivative is determined which defines the loading variations for small ($\alpha \leq 5^\circ$) angle of attack perturbations. No attempt is made to fit higher order approximations or piecewise linear functions to the nonlinear load variations; at the present time, these are simply identified as nonlinearities. The results of this analysis for the PIPER are shown in Tables 3 and 4; a representative case of the tapered wings ($\lambda = 0.5$, winglets down) is shown in Table 5.

Several characteristics of the MAV flight regime are apparent from the tabulated data. As expected, the most significant derivative is the lift curve slope, which is linear in the range of angles of attack tested and does not vary greatly

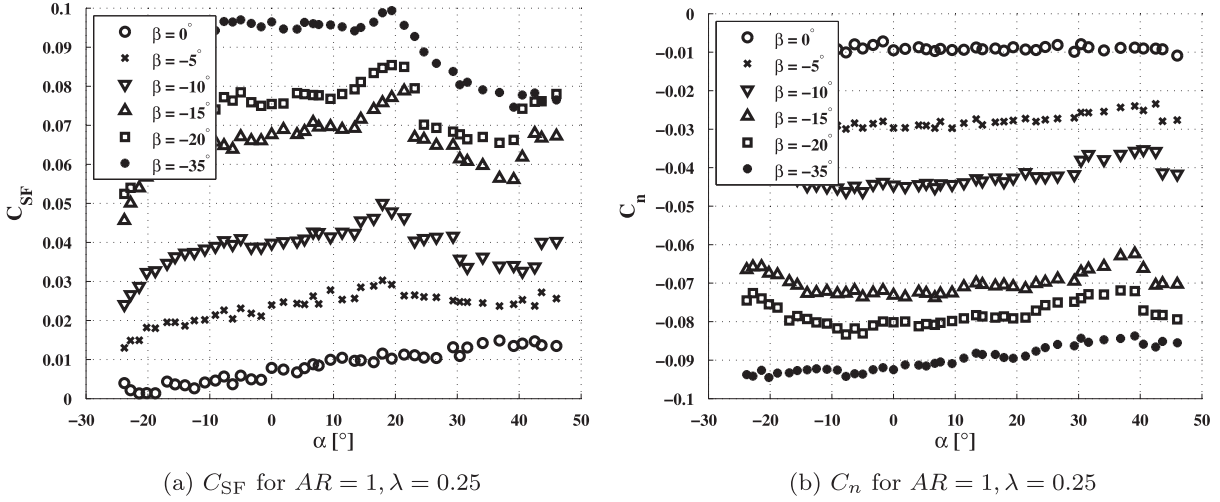


Figure 7. Side force (C_{SF}) and yaw moment (C_n) coefficients for selected flat plate wings in sideslip at $Re = 7.5 \times 10^4$.

Table 3. $\partial/\partial\alpha$ derivatives for the tailless PIPER MAV at $Re = 7.5 \times 10^4$; configurations not well approximated by a constant stability derivative (linear gradient) for all $5^\circ \leq \alpha \leq 15^\circ$ are labeled 'NL' (nonlinear).

Derivative	$\beta = 0^\circ$	$\beta = -5^\circ$	$\beta = -10^\circ$	$\beta = -15^\circ$	$\beta = -20^\circ$
$C_{L,\alpha}$	2.02	1.99	1.91	1.76	1.81
$C_{D,\alpha}$	0.544	0.578	0.547	0.510	0.541
$C_{M,\alpha}$	-0.185	NL	-0.182	-0.178	-0.205
$C_{l,\alpha}$	-0.028	NL	0.051	0.093	0.098
$C_{n,\alpha}$	NL	0.0187	NL	NL	NL
$C_{SF,\alpha}$	NL	-0.0616	NL	NL	NL

Table 4. $\partial/\partial\alpha$ derivatives for the PIPER MAV with tail surfaces at $Re = 7.5 \times 10^4$; configurations not well approximated by a constant stability derivative (linear gradient) for all $5^\circ \leq \alpha \leq 15^\circ$ are labeled 'NL' (nonlinear).

Derivative	$\beta = 0^\circ$	$\beta = -5^\circ$	$\beta = -10^\circ$	$\beta = -15^\circ$	$\beta = -20^\circ$
$C_{L,\alpha}$	2.57	2.53	2.69	2.67	2.59
$C_{D,\alpha}$	0.730	0.764	0.758	0.716	0.669
$C_{M,\alpha}$	NL	-0.292	-0.341	-0.371	-0.394
$C_{l,\alpha}$	NL	NL	NL	NL	NL
$C_{n,\alpha}$	NL	NL	0.0281	NL	NL
$C_{SF,\alpha}$	NL	NL	-0.0917	NL	NL

Table 5. $\partial/\partial\alpha$ derivatives for the $\lambda = 0.5$ wing with winglets down at $Re = 7.5 \times 10^4$; configurations not well approximated by a constant stability derivative (linear gradient) for all $5^\circ \leq \alpha \leq 15^\circ$ are labeled 'NL' (nonlinear).

Derivative	$\beta = 0^\circ$	$\beta = -5^\circ$	$\beta = -10^\circ$	$\beta = -15^\circ$	$\beta = -20^\circ$
$C_{L,\alpha}$	2.41	2.39	2.37	2.30	2.32
$C_{D,\alpha}$	1.10	1.09	1.07	1.03	1.01
$C_{M,\alpha}$	NL	NL	NL	NL	NL
$C_{l,\alpha}$	NL	0.042	0.066	0.104	0.166
$C_{n,\alpha}$	NL	NL	NL	-0.0504	-0.0486
$C_{SF,\alpha}$	-0.0526	NL	0.0576	0.120	NL

with increasing sideslip angle. While the drag coefficient and most of the pitching moment configurations are also linear about the cruise condition, it is also clear that the

majority of the lateral derivatives ($C_{l,\alpha}$, $C_{n,\alpha}$, $C_{SF,\alpha}$) are typically not well represented by a linear fit. This is of little significance for the yaw and side force derivatives; the few

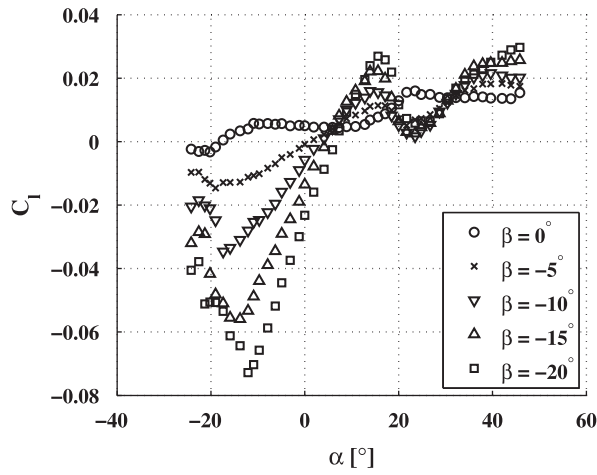
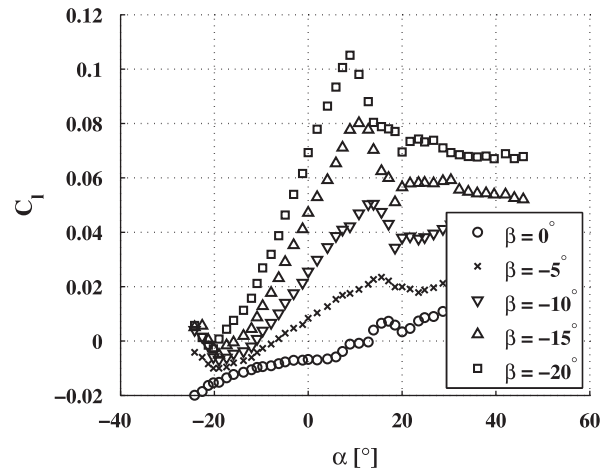
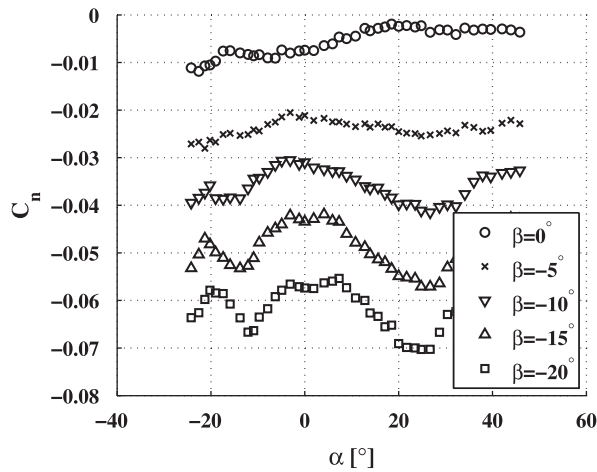
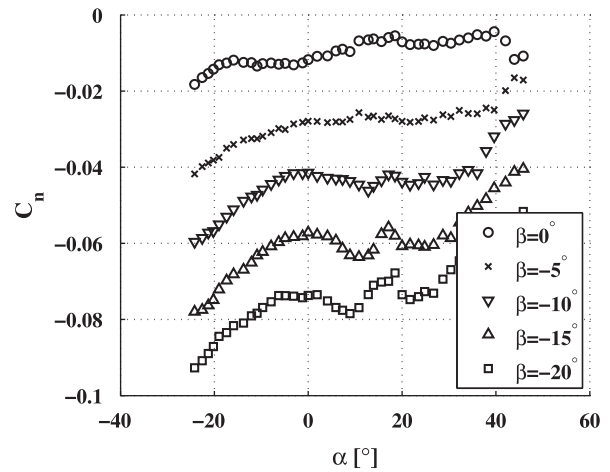
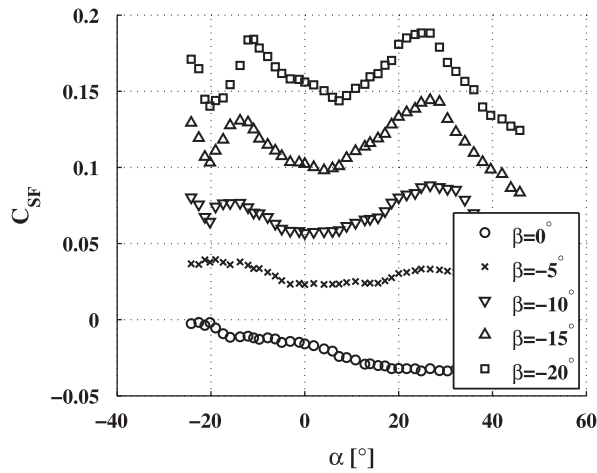
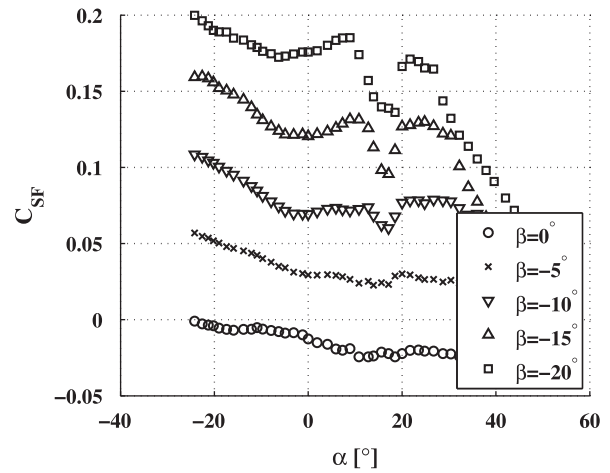
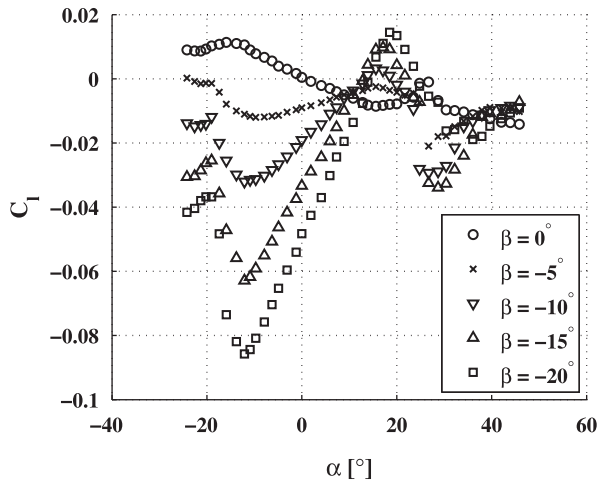
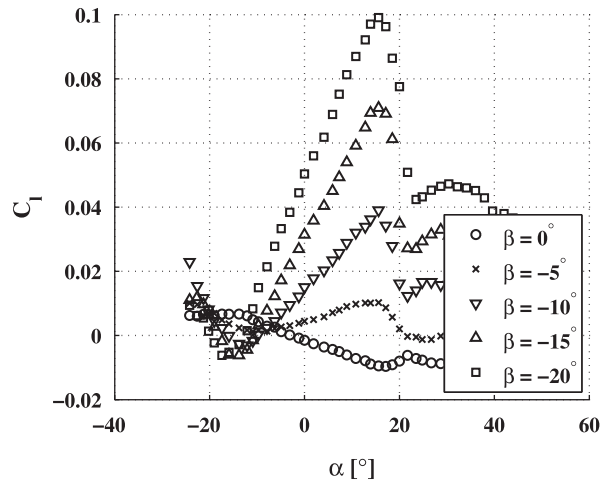
(a) C_l for $AR = 1, \lambda = .5$, winglets down(b) C_l for $AR = 1, \lambda = .5$, winglets up(c) C_n for $AR = 1, \lambda = .5$, winglets down(d) C_n for $AR = 1, \lambda = .5$, winglets up(e) C_{SF} for $AR = 1, \lambda = .5$, winglets down(f) C_{SF} for $AR = 1, \lambda = .5$, winglets up

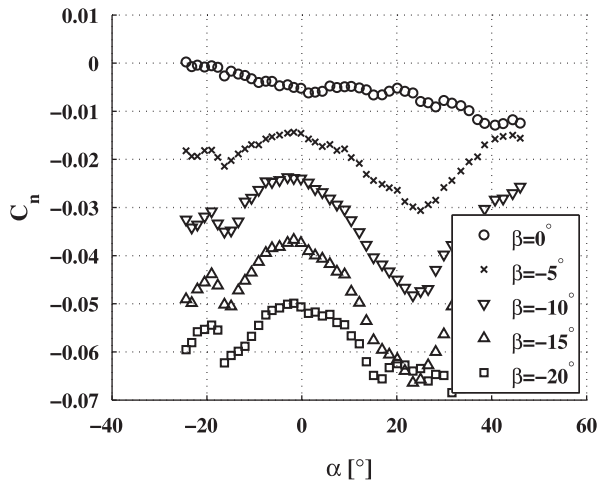
Figure 8. Roll moment (C_l), yaw moment (C_n) and side force (C_{SF}) coefficients for $\lambda = 0.5$ flat plate wings in sideslip at $Re = 7.5 \times 10^4$ with varying winglet configurations.



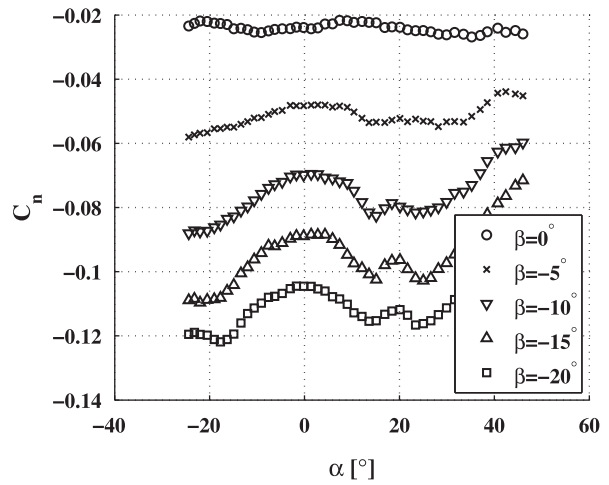
(a) C_l for $AR = 1, \lambda = .75$, winglets down



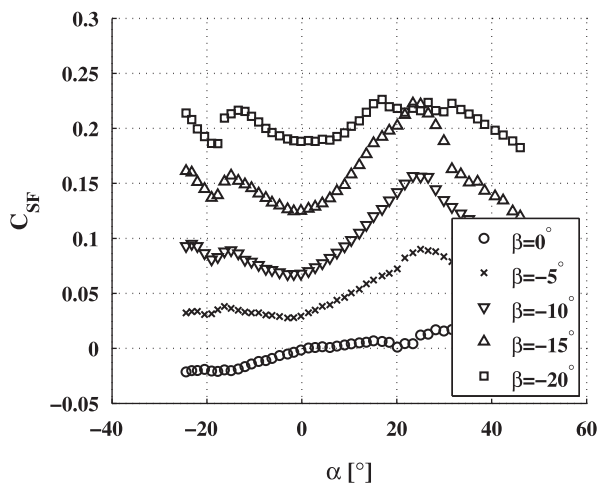
(b) C_l for $AR = 1, \lambda = .75$, winglets up



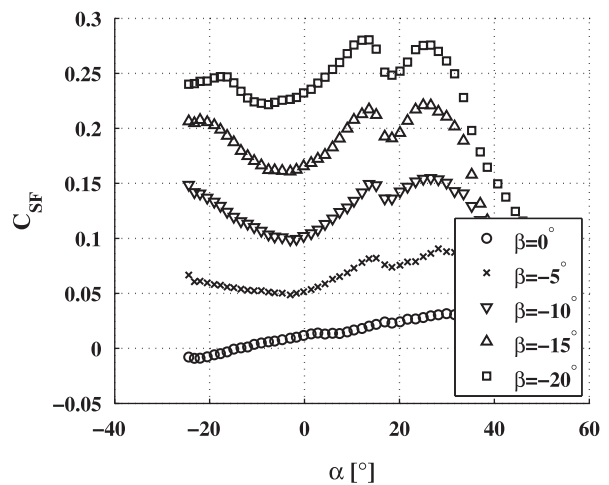
(c) C_n for $AR = 1, \lambda = .75$, winglets down



(d) C_n for $AR = 1, \lambda = .75$, winglets up



(e) C_{SF} for $AR = 1, \lambda = .75$, winglets down



(f) C_{SF} for $AR = 1, \lambda = .75$, winglets up

Figure 9. Roll moment (C_l), yaw moment (C_n) and side force (C_{SF}) coefficients for $\lambda = 0.75$ flat plate wings in sideslip at $Re = 7.5 \times 10^4$ with varying winglet configurations.

available values in Tables 3 and 5 are two orders of magnitude lower than the lift curve slope, as would be expected from the small magnitudes seen in the plots in Sections 3.1 and 3.2. Thus, these derivatives can likely be neglected. The case of the roll moment, however, is significant as it pertains to the axis with the smallest associated moments of inertia. The prescribed range of angle of attack allows a valid linear approximation leading up to the roll stall; however, for the PIPER with vertical tails attached, a more drastic roll stall occurs at a slightly lower angle of attack and disrupts the linearity of the $C_{l,\alpha}$ stability derivative (as seen in Figure 5(a)). This result invalidates the aforementioned assumption of decoupling the lateral and longitudinal loads; for a MAV flying at even a small sideslip angle of $\beta = -5^\circ$, a small angle of attack perturbation can induce a significant, and potentially nonlinear, variation in roll moment. One can also envision the contribution of this derivative to a Dutch-roll type instability in which coupled sideslip and angle of attack perturbations can result in strongly destabilizing roll moments.[33]

3.4. Stability derivatives due to sideslip angle

While the cross-coupled stability derivative $C_{l,\alpha}$ is seen to be significant for the PIPER MAV (and the canonical tapered wing test cases), the roll stability derivative $C_{l,\beta}$ is typically of more concern for MAV control as the magnitude is even larger. In addition, MAVs are known to be especially sensitive to lateral perturbations due to their small moments of inertia in the lateral plane; thus, a similar force variation may be more significant when applied laterally to a LAR wing. Computation of this value involves choosing a trim angle of attack and then determining the variation in roll moment with respect to the range of sideslip angles tested ($-20^\circ \leq \beta \leq 0^\circ$). It was found that $C_{l,\beta}$ could be linearly represented up to a sideslip angle of $\beta = -15^\circ$; larger perturbations of $\beta = -20^\circ$ resulted in some nonlinearities. Previous results by the authors reported the value of $C_{l,\beta}$ for the tapered wings (and additional geometries) tested in this investigation at various equilibrium angles of attack; the values are reproduced in Table 6. The results of the previous sections showed the contribution of the winglets to reducing the roll moment at positive angles of attack; the corresponding values of $C_{l,\beta}$ at equilibrium angles of $\alpha_{\text{trim}} = 10^\circ$ and 20° are given in Table 7 along with $C_{n,\beta}$ and $C_{SF,\beta}$ for comparison.

The most significant result obtained from the testing is the effectiveness of the winglets-down configuration in reducing the roll stability derivative. This can be attributed to two different effects; first, the incident flow on the winglets creates a negative roll moment when the winglets are below the center of gravity of the wing (and a positive roll moment for the winglets-up configuration, similar to the MAV with the tails attached). Second, the downward configuration is more effective at preventing the development of the tip vortices

and their resulting effects on the aerodynamic loading.[14] As a result, the tip vortex asymmetry and the ensuing roll moment are mitigated. At a trim angle of attack of $\alpha_{\text{trim}} = 10^\circ$, the winglets down configuration creates a reduction in $C_{l,\beta}$ by 55% and 44% for the $\lambda = 0.5$ and $\lambda = 0.75$ configurations and an effective elimination of the derivative for $\lambda = 0.25$. While the winglets-up configuration actually increases the value of $C_{l,\beta}$ (for the same physical reasons just described for the winglet-down geometry), the reduction in the roll stability derivative with the addition of winglets centered below the wing shows great promise for increased lateral stability for MAVs. It should also be noted that the addition of these winglets does not adversely affect the longitudinal loading or derivatives, particularly in the range of reasonable flight regimes for a MAV, and thus can be used to improve lateral stability without incurring a significant penalty in lift.

The derivatives $C_{n,\beta}$ and $C_{SF,\beta}$ are also affected by the presence of the winglets; however, this has less to do with the disruption of the tip vortices than it does with the force generated by the flow around the winglet. The results in Table 7 indicate that the weathercock derivative $C_{n,\beta}$ is always positive and, while some variation between the winglets-up and -down configurations is noticeable, it is not the order of magnitude variation seen with the roll stability derivative. Similarly, $C_{SF,\beta}$ is always negative and the values for a given wing do not change significantly. This indicates that the winglets behave like conventional tail surfaces by providing a positive yaw moment and negative side force during a negative sideslip perturbation. While $C_{SF,\beta}$ does not contribute greatly to the stability of the vehicle, the positive values of $C_{n,\beta}$ provide a restoring moment for the MAV whether they are placed above or below the wing. Thus, the addition of a winglet below the wing can reduce the roll stability derivative to manageable levels while improving the yaw stability and not affecting the longitudinal loads.

4. Discussion

The results of the previous section indicate the inherent complexity involved with the stability and control of MAVs, which exhibit coupled loading between lateral and longitudinal axes as well as significant magnitude control derivatives which arise from the unique flow phenomena associated with LAR wings. It is instructive to consider how these loads may arise in the context of MAV flight in order to consider the practical implications of the results shown in the previous section. The authors' flight testing experience with MAVs and other low Reynolds number aircraft [5,27] has indicated the propensity to become unstable due to perturbations in sideslip. The significance of the $C_{l,\beta}$ derivative provides an explanation. A small increase in sideslip angle, which could be created by a lateral gust, aerodynamically creates a roll moment into the direction of the wind. While a negative value of the roll stability derivative is typically

Table 6. Values of $C_{l,\beta}$ for various planform geometries and trim angles.

Planform	$\alpha = 5^\circ$	$\alpha = 10^\circ$	$\alpha = 15^\circ$	$\alpha = 20^\circ$
AR=0.75 $\lambda = 1$	-0.062	-0.106	-0.161	-0.233
AR=1 $\lambda = 1$	-0.101	-0.167	-0.238	-0.313
AR=1.5 $\lambda = 1$	-0.053	-0.086	-0.123	-0.177
AR=3 $\lambda = 1$	-0.019	-0.048	-0.105	-0.179
AR=1 $\lambda = 0.75$	-0.047	-0.086	-0.150	-0.173
AR=1 $\lambda = 0.5$	-0.057	-0.088	-0.105	-0.128
AR=1 $\lambda = 0.25$	-0.036	-0.055	-0.067	-0.051

Table 7. Lateral stability derivatives due to β for varying configurations.

	PIPER (no tail)	PIPER (with tail)	$\lambda = 0.25$ (w/l down)	$\lambda = 0.25$ (w/l up)	$\lambda = 0.5$ (w/l down)	$\lambda = 0.5$ (w/l up)	$\lambda = 0.75$ (w/l down)	$\lambda = 0.75$ (w/l up)
$\alpha_{\text{trim}} = 10^\circ$	-0.198	-0.381	0.0007	-0.144	$C_{l,\beta}$ -0.039	-0.288	-0.048	-0.28
$\alpha_{\text{trim}} = 20^\circ$	-0.212	-0.27	-0.017	-0.088	0.023	-0.19	0.021	-0.126
$\alpha_{\text{trim}} = 10^\circ$	0.006	0.354	0.176	0.149	$C_{n,\beta}$ 0.162	0.217	0.162	0.287
$\alpha_{\text{trim}} = 20^\circ$	0.038	0.217	0.181	0.132	0.198	0.203	0.215	0.281
$\alpha_{\text{trim}} = 10^\circ$	-0.184	-1.08	-0.393	-0.305	$C_{SF,\beta}$ -0.516	-0.592	-0.584	-0.727
$\alpha_{\text{trim}} = 20^\circ$	-0.324	-0.785	-0.396	-0.28	-0.625	-0.566	-0.772	-0.667

considered stabilizing, the magnitude of $C_{l,\beta}$ as presented in this study will present control problems and potentially cause instability. This flow behavior will develop regardless of the size of the vertical tail surfaces (although the magnitude and dynamics may increase with larger tails) because of the inherent asymmetry in the tip vortices. The significance of the $C_{l,\alpha}$ cross-coupled derivative indicates that this undesirable effect will be augmented by any simultaneous increases in angle of attack. This will create the lateral asymmetries that a MAV, with its low moments of inertia, has difficulty overcoming.

It is instructive to compare the magnitude of the $C_{l,\beta}$ derivative (and others) with more conventional aircraft to consider the impact of roll stall on MAV control. Tabulated values for a variety of aircraft can be found in aircraft dynamics textbooks [32,34] and are reproduced in Table 8 for comparison. It is apparent that while the lift curve slope is significantly higher for a Boeing 747 (for example) than the PIPER MAV, the roll stability derivatives exhibit similar magnitudes. It is surprising to note that this is still the case for the tapered wings, which have no vertical geometry to impact the lateral stability; in fact, the entire effect can be attributed to the asymmetric aerodynamics associated

with the LAR wing. The inclusion of downward winglets for the tapered wings reduced the value of $C_{l,\beta}$ to near the magnitude of a laterally stable aircraft. Finally, it should be noted that cross-coupled derivatives such as $C_{l,\alpha}$ are not listed in these textbooks as they are not relevant for larger aspect ratio wings; however, the results of this paper show that is not necessarily the case for MAVs.

While the large magnitude of $C_{l,\beta}$ is clearly of importance in the lateral control of LAR fliers, it is encouraging that the effectiveness of the downward winglets in reducing the magnitude of the roll stability derivative by up to an order of magnitude in some cases suggests a potential new control strategy. While some groups have studied the effects of longitudinally flexible membrane wings for the purpose of reducing lift perturbations during a gust,[4] the implications of a vertical geometry located at the edge of the wing are that lateral stability could be increased by flexing the wingtip downwards by reducing the $C_{l,\beta}$ derivative. MAVs have difficulty with traditional control surfaces due to the separated flow over the suction side of the wing; while this reduces the effectiveness of ailerons located at the trailing edge of the wing, it would not alter the impact of the winglets. This concept is diagrammed in Figure 10, which shows how

Table 8. Stability derivatives of conventional aircraft.[32,34]

	$C_{L,\alpha}$	$C_{D,\alpha}$	$C_{M,\alpha}$	$C_{l,\beta}$	$C_{n,\beta}$	$C_{SF,\beta}$
Boeing 747-100	5.70	0.66	-1.26	-0.221	0.150	-0.96
McDonnell-Douglas DC-8	4.81	0.487	-1.478	-0.158	0.1633	-0.8727
Convair CV-880M	4.66	0.43	-0.381	-0.239	0.145	-1.011
PIPER MAV (no tails, $\alpha_{trim} = 10^\circ$)	2.02	0.544	-0.185	-0.198	0.00641	-0.184
PIPER MAV (with tails, $\alpha_{trim} = 10^\circ$)	2.57	0.730	'NL'	-0.381	0.354	-1.07

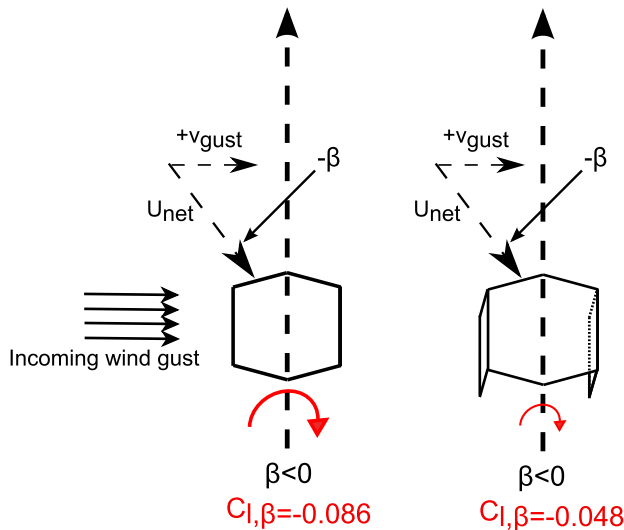


Figure 10. A potential lateral instability due to roll stall: a sideways gust induces a nonzero $C_{l,\beta}$ which is reduced by the presence of downward oriented winglets.

lateral gusts alter the instantaneous sideslip angle of a flying wing. With the winglet configuration below the wing, as seen on the right, $C_{l,\beta}$ is reduced and the aircraft can better withstand a gust perturbation.

5. Conclusions

This paper has experimentally investigated the static lateral loads experienced by small wingspan aircraft, and specifically the PIPER MAV which has been developed by the group. By using wind tunnel testing to measure the roll moment, yaw moment, and side force (in addition to the longitudinal loads), static stability derivatives were computed and used to describe some of the most significant control challenges of MAVs. The roll stability derivative was seen to be dependent upon the tip vortex asymmetry in sideslip and demonstrates the susceptibility of these vehicles to lateral gusts. In addition, the roll moment was observed to vary with angle of attack as well as sideslip; this leads to the existence of the cross-coupled derivative $C_{l,\alpha}$, which shows the interaction between lateral loads and longitudinal

perturbations for MAVs. Finally, by adding winglets to the edges of tapered wings in a configuration hanging below the center of gravity of the wing, the magnitude of $C_{l,\beta}$ can be reduced by 55% and 44% for the $\lambda = 0.5$ and $\lambda = 0.75$ wings, respectively; for the smallest taper ratio of 0.25, the roll moment was effectively eliminated. These effects do vary with the equilibrium (or ‘cruise’) flight angle, but they demonstrate the significance of tip vortex asymmetry on the lateral loading and stability of MAVs.

Notes on contributors



Matt Shields is a graduate research assistant working in Dr. Kamran Mohseni’s group at the University of Florida. He received his BS/MS in Aerospace Engineering Sciences from the University of Colorado in 2010, where he began working on the group’s Micro Aerial Vehicle project. After successfully designing a flying aircraft, Matt has focused on developing the Prototunnel for the use of low Reynolds number, low aspect ratio aerodynamics testing with the goal of characterizing how the propagation of three dimensional flow phenomena has a dominant effect on the stability and control of MAVs. This understanding can be used to develop better controllers and design more efficient vehicles.



Kamran Mohseni is the W.P. Bushnell Endowed Chair and a Professor in Mechanical & Aerospace Engineering Department and Electrical & Computer Engineering at the University of Florida in Gainesville. He received his B.S. degree from the University of Science and Technology, Tehran, Iran; his M.S. degree in Aeronautics and Applied Mathematics from the Imperial College of Science, Technology, and Medicine, London, U.K.; and his Ph.D. degree in Mechanical Engineering from the California Institute of Technology (Caltech), Pasadena, in 2000. He was a Postdoctoral Fellow in Control and Dynamical Systems with Caltech. In 2001, he joined the University of Colorado at Boulder, where he rose to the rank of Associate Professor in Aerospace Engineering Sciences before transferring to Florida in 2011. His research interests include aerial and underwater vehicle control, mobile sensor networking, microscale transport, vortex dynamics, and biomimetic and fluidic locomotion. Dr. Mohseni is a member of the American Society of Mechanical Engineers, Institute of Electrical and Electronics Engineers, American Physical Society, and the Society for Industrial and Applied Mathematics. He is an Associate Fellow of the American Institute of Aeronautics and Astronautics.

References

- [1] J Grasmeyer, M Keennon. Development of the Black Widow micro air vehicle. AIAA paper 2001-0127, Reno, NV, 2001, 39th AIAA Aerospace Sciences Meeting & Exhibit.
- [2] R Hundley, E Gritton. Future technology-driven revolutions in military operations. RAND Corporation Document No. DB-110-ARPA, 1994.
- [3] R Wasak, D Jenkins, P Ifju. Stability and control properties of an aeroelastic fixed wing micro aerial vehicle. AIAA paper 2002-4005; 2001.
- [4] Ifju P, Jenkins D, Ettinger S, Lian Y, Shyy W, Waszak M, Flexible-wing-based micro air vehicles. AIAA paper 2002-0705, 40th Aerospace Sciences Meeting & Exhibit. Nevada: Reno; January 2002.
- [5] M Shields, K Mohseni. Static aerodynamic loading and stability considerations for a micro aerial vehicle. AIAA paper 2010-4389, 28th AIAA Applied Aerodynamics Conference, Chicago, IL; June 28-July 1 2010.
- [6] Arena A, Mueller T. Laminar separation, transition, and turbulent reattachment near the leading edge of airfoils. AIAA J. 1980;18(5):747-753.
- [7] Brendel M, Mueller T. Boundary-layer measurements on an airfoil at low reynolds numbers. J. Aircraft. 1988;25(7):612-617.
- [8] Taira K, Colonius T. Three-dimensional flows around low-aspect-ratio flat-plate wings at low reynolds numbers. J. Fluid Mech. 2009;623:187-207.
- [9] Swanton E, Vanier B, Mohseni K. Flow visualization and wall shear stress of a flapping model hummingbird wing. Exp. Fluids. 2010;49:657-671.
- [10] Williams D, Quach V, Kerstens W, Buntain S, Tadmor G, Rowley C, Colonius T. Low-reynolds number wing response to an oscillating freestream with and without feed forward control. Proceedings of the 47th AIAA Aerospace Sciences Meeting including the New Horizons Forum and Aerospace Exposition, AIAA, Orlando, FL, 2009, AIAA paper 2009-143.
- [11] Williams D, Tadmor G, Colonius T, Kerstens W, Quach V, Buntain S. Lift response of a stalled wing to pulsatile disturbances. AIAA J. 2009;47:3031-3037.
- [12] Pelletier A, Mueller T. Low reynolds number aerodynamics of low-aspect-ratio, thin/flat/cambered-plate wings. J. Aircraft. 2000;37:825-832.
- [13] Torres G, Mueller T. Low-aspect-ratio wing aerodynamics at low reynolds numbers. AIAA J. 2004;42:865-873.
- [14] Shields M, Mohseni K. Effects of sideslip on the aerodynamics of low-aspect-ratio low-reynolds-number wings. AIAA J. 2012;50:85-99.
- [15] Lam K, Leung M. Asymmetric vortex shedding flow past an inclined flat plate at high incidence,". Eur. J. Mech. B-Fluids. 2005;24:33-48.
- [16] Jian T, Ke-Qin Z. Numerical and experimental study of flow structure of low aspect ratio wing. J. Aircraft. 2004;41:1196-1201.
- [17] Gresham N, Wang Z, Gursul I. Low Reynolds number aerodynamics of free-to-roll low aspect ratio wings. Exp. Fluids.. 2010;49:11-25.
- [18] Lamar J. Prediction of vortex flow characteristics of wings at subsonic and supersonic speeds. J. Aircraft. 1975;13:490-494.
- [19] Hall M. A theory for the core of a leading-edge vortex. J. Fluid Mech. 1961;11:209-228.
- [20] Mueller T, Delaurier J. Aerodynamics of small vehicles. Ann. Rev. Fluid Mech. 2003;35:89-111.
- [21] Shyy W, Lian Y, Tang J, Viieru D, Liu H. Aerodynamics of low Reynolds number flyers. New York (NY): Cambridge Aerospace Series; 2008.
- [22] Phillips W. Mechanics of flight, 2nd ed. Hoboken (NJ): John Wiley & Sons; 2010.
- [23] Lawrence D, Mohseni K, Han R. Information energy for sensor-reactive UAV flock control. AIAA paper 2004-6530, 3rd AIAA Unmanned Unlimited Technical Conference, Workshop and Exhibit. September 2004 20-23; Chicago, IL.
- [24] Allred J, Hasan A, Pisano B, Panichsakul S, Gray P, Han R, Lawrence D, Mohseni K. SensorFlock: a mobile system of networked micro-air vehicles. The ACM SenSys 2007: The 5th ACM Conference on Embedded Networked Sensor Systems. 2007 November 6-9, Sydney.
- [25] Shaw A, Mohseni K. A fluid dynamic based coordination of a wireless sensor network of unmanned aerial vehicles: 3-D simulation and wireless communication characterization. IEEE Sensors Journal, Special Issue on Cognitive Sensor Networks. March 2011;11:722-736.
- [26] Hall J, Lawrence D, Mohseni K. Lateral control of a tailless micro aerial vehicle, AIAA paper 2006-6689, AIAA Guidance, Navigation, and Control Conference and Exhibit. Colorado, Keystone; 2006 August 21-24.
- [27] Hodgkinson B, Lipinski D, Peng L, Mohseni K. High resolution atmospheric sensing using UAV swarms. Accepted to International Symposium on Distributed Autonomous Robotic, System DARS2012; 2012.
- [28] Shields M, Mohseni K. The development of roll stall for low aspect ratio wings. J. Aircraft. Accepted for publication.
- [29] Shields M, Mohseni K. The influence of roll stall on the lateral control of micro aerial vehicles. AIAA paper 2012-4462, AIAA Guidance Navigation and Control Conference, Minneapolis, MN; 2012 August 13-16.
- [30] Calibration and Use of Internal Strain-Gage Balances with Application to Wind Tunnel Testing, AIAA recommended practice R-091-2003, AIAA, Alexander Bell Drive, Suite 500. Reston, VA. 1801; 20191; 2003.
- [31] Rae W, Pope A. Low-speed wind tunnel testing. 2nd ed. New York: John Wiley & Sons; 1984.
- [32] Schmidt L. Introduction to aircraft flight dynamics. Reston (VA): AIAA; 1998.
- [33] Phillips W, Niewoehner R. Characteristic length and dynamic time scale associated with aircraft pitching motion. J. Aircraft. 2009;46:572-582.
- [34] Nelson R. Flight stability and automatic controls. New York, NY: McGraw-Hill Co.; 1989.